Strength of an Interloop Hydrogen Bond Determines the Kinetic Pathway in Catalysis by *Escherichia coli* Dihydrofolate Reductase†

Grover Paul Miller‡ and Stephen J. Benkovic*

Department of Chemistry, The Pennsylvania State University, University Park, Pennsylvania 16802

Received December 12, 1997; Revised Manuscript Received March 6, 1998

ABSTRACT: On the basis of X-ray crystallographic data, Sawaya and Kraut proposed that Met20 loop conformational changes modulate ligand specificity observed in the catalytic cycle for *Escherichia coli* dihydrofolate reductase (DHFR) [Sawaya, M. R., and Kraut, J. (1997) *Biochemistry 36,* 586−603]. Interloop hydrogen bonds stabilize either a closed Met20 loop conformation observed in substrate complexes or an occluded Met20 loop conformation observed in product complexes, respectively. To test this model, we targeted a single hydrogen bond occurring exclusively in the closed Met20 loop conformation. Specifically, Asp122 in the βF−βG loop was independently substituted with asparagine, serine, and alanine—amino acids with decreasing abilities to hydrogen-bond. The kinetic analyses of the Asp122 mutants enabled the construction of kinetic schemes at pH 7.0 that demonstrate two striking features. First, a significant correlation exists between decreased binding of nicotinamide adenine dinucleotide phosphate, reduced (NADPH), and decreased hydride transfer rates resulting from these mutations. In other words, the interactions of Asp122 are along the reaction coordinate leading to the transition state. Second, substitutions for Asp122 alter the catalytic pathway preferred by wild-type DHFR under saturating conditions of substrate and cofactor. Overall, the steady-state rate contains contributions from the product off rates from the DHFR·5,6,7,8-tetrahydrofolate (H_4F) and DHFR·NADPH·H_4F complexes and from the rate of hydride transfer. These mutational effects support the mechanistic model whereby interloop contacts regulate an equilibrium of Met20 loop conformations that, in turn, modulate ligand affinity and turnover.

Due to the wealth of crystallographic (ref *1* and references therein) and solution structure information (*2*−*4*) and of kinetic (*5*) and computational analyses (*6*), dihydrofolate reductase (5,6,7,8-tetrahydrofolate:$NADP^+$ oxidoreductase, EC 1.5.1.3; DHFR)[1] is an ideal candidate for studying elements of catalysis. For example, as observed for many other enzymes, catalysis by DHFR is limited by physical rather than chemical processes (*7*). DHFR utilizes NADPH to reduce 7,8-dihydrofolate (H_2F) to 5,6,7,8-tetrahydrofolate (H_4F), an important metabolite involved in the biosynthesis of purines, thymidylate, and several amino acids. At neutral pH, the flux of substrate through the DHFR catalytic cycle is limited by the rate of product formation rather than the rate of hydride transfer. Unlike eukaryotic cells, where the concentration of $NADP^+$ is no more than 1% that of NADPH, prokaryotic cells have comparable levels of $NADP^+$ and NADPH (*8*). To reduce dihydrofolate under these conditions, DHFR has evolved a catalytic cycle relying on the binding of NADPH to accelerate product (H_4F) release. Ultimately, DHFR cycles through five kinetically observable intermediates to complete one catalytic cycle (*5*).

A recent publication of isomorphous X-ray crystal structures indicates that domain rotation and interloop interactions are key features differentiating liganded complexes of DHFR (*1*). On the basis of these structures, Sawaya and Kraut propose that conformational changes suggested by these data can account for alterations in ligand specificity observed in the kinetic mechanism (*5*). Domain rotation opens and closes the active-site cleft to facilitate binding and release of ligands. Another striking observation is the presence of two ligand-dependent conformations of the Met20 loop. A closed conformation occurs in the formation of DHFR·NADPH and the Michaelis complex (DHFR·NADPH·H_2F), and an occluded conformation, where the Met20 loop occupies part of the cofactor binding site, occurs in the DHFR·$NADP^+$·H_4F, DHFR·H_4F, and DHFR·NADPH·H_4F complexes. The preference of the Met20 loop conformations in either substrate or product complexes posits a functional role for Met20 loop flexibility.

An important distinction between the Met20 conformations is the positioning of residues Glu17−Met20. In the closed conformation observed in substrate complexes, this portion of the Met20 loop forms a short antiparallel sheet and type III′ hairpin turn, which extends across and seals the active site. For product complexes, the central part of the Met20

† This work was supported in part by NIH Grant GM24129.

* To whom correspondence should be addressed: Tel 814-865-2882; Fax 814-865-2973; email sjb1@psu.edu.

‡ Recipient of Homer F. Braddock College of Science Memorial Scholarship.

[1] Abbreviations: DHFR, dihydrofolate reductase; MTX, methotrexate; H_2F, 7,8-dihydrofolate; H_4F, 5,6,7,8-tetrahydrofolate; NADPH or NH, nicotinamide adenine dinucleotide phosphate, reduced; NADPD, [(4′*R*)-^{2}H]nicotinamide adenine dinucleotide phosphate, reduced; DNADPH, 5,6-dihydro-nicotinamide adenine dinucleotide phosphate, reduced; $NADP^+$ or N^+, nicotinamide adenine dinucleotide phosphate, oxidized; ^DV, $k_{hyd,NADPH}/k_{hyd,NADPD}$; EDTA, ethylenediaminetetraacetic acid; DTT, dithiothreitol.

S0006-2960(97)03065-1 CCC: $15.00
Published on Web 04/18/1998

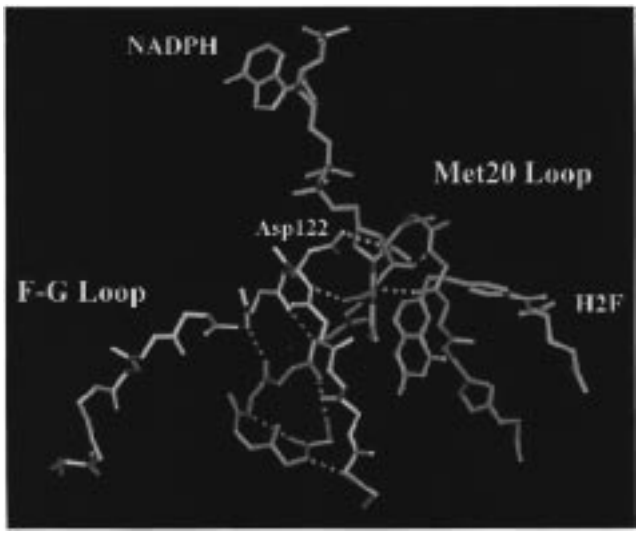

FIGURE 1: The closed Met20 loop requires interactions with the βF−βG loop. For simplicity only the Met20 (blue) and βF−βG loops (yellow) are shown in relation to ligands (green). The crystal structure of the DHFR·$NADP^+$·folate complex (*1*) was used to construct this figure using QUANTA.

loop forms a 3_{10} helix, which occludes the binding site for the nicotinamide ring of the cofactor. The stabilization of these Met20 conformers involves hydrogen-bonding interactions with an outer loop, specifically the βF−βG loop in substrate complexes and the βG−βH loop in product complexes. Alteration of the outer loops would conceivably affect Met20 loop dynamics reflected in destabilized substrate or product complexes.

Specific contacts between the βF−βG and Met20 loops include both the protein backbone and side chain of Asp122 (Figure 1). Backbone−backbone hydrogen bonds between the loops are the dominant stabilizing contacts. The sole side chain−backbone hydrogen bond involves the side chain of Asp122 of the βF−βG loop and the backbone amide of Glu17 of the Met20 loop. Evolutionary bias for Asp122 is observed for all prokaryotic DHFRs, suggesting the importance of a short acid side chain at this position. Even though these bonds form, these interactions must not impede formation of the transient conformations of the Met20 loop. To accomplish intermittent contacts, the βF−βG loop may also require conformational flexibility. High *B*-factors, corresponding to this loop found in X-ray crystal structures, are consistent with this proposal (*9*). Moreover, a glycine (Gly121) located in the center of this loop displays significant backbone flexibility from an NMR study of the DHFR·folate complex (*4*).

To assess the importance of interloop interactions modulating Met20 loop conformations, we constructed a series of mutants of the βF−βG loop and characterized them kinetically. To alter a specific contact between the loops, Asp122 was independently substituted with asparagine, serine, and alanine—amino acids with decreasing abilities to hydrogen-bond. Weakening the side-chain contacts between the βF−βG and Met20 loops would make the closed conformation of the Met20 loop less favorable. Since Asp122 does not form any interprotein contacts in the occluded conformation, the substitutions of Asp122 should not affect product complexes. If the model for alternating Met20 loop conformations proposed by Sawaya and Kraut proves appropriate, then these mutations would decrease the stability of substrate complexes and potentially affect formation of the transition-state complex.

MATERIALS AND METHODS

Materials. All reagents were purchased from Fisher Scientific or Sigma Chemical Co. Propagation of plasmid DNA was carried out using *Escherichia coli* DH5α cells. Restriction and DNA modifying enzymes were purchased from New England Biolabs. Oligonucleotides for mutagenesis were synthesized on a 8909 Perceptive Biosystems DNA synthesizer. All assays were conducted with the buffer MTEN [50 mM MES [2-(*N*-morpholino)ethanesulfonic acid], 25 mM Tris [tris(hydroxymethyl)aminomethane], 25 mM ethanolamine, and 100 mM NaCl] at 25 °C. The pH of this buffer was adjusted to pH 7.0 or 9.0, depending on the design of the experiment.

Preparation of DHFR Ligands. The substrate, dihydrofolate (H_2F), was prepared from folic acid by dithionite reduction (*10*), whereas the product, (6*S*)-tetrahydrofolate (H_4F), was prepared from H_2F by using *E. coli* dihydrofolate reductase (*11*). NADPH and $NADP^+$ were purchased from Sigma. The cofactor, [4′(R)-^{2}H]NADPH (NADPD), was prepared by using alcohol dehydrogenase from *Leuconostoc mesenteroides* to reduce $NADP^+$ as described by Viola et al. (*12*). Synthesis of 5,6-dihydro-NADPH (DNADPH) was accomplished by reduction of NADPH under 1 atm of hydrogen with a palladium−carbon catalyst (*13*). The following extinction coefficients were used to determine the concentrations of ligand solutions: H_2F, 28 mM^{-1} cm^{-1} at 282 nm, pH 7.4 (*14*); H_4F, 28 mM^{-1} cm^{-1} at 297 nm, pH 7.5 (*15*); MTX, 22.1 mM^{-1} cm^{-1} at 302 nm in 0.1 M KOH (*16*); NADPH (NADPD), 6.22 mM^{-1} cm^{-1} at 340 nm, pH 7.0 (*17*); $NADP^+$, 18 mM^{-1} cm^{-1} at 259 nm, pH 7.0 (*17*); DNADPH, 18 mM^{-1} cm^{-1} at 259 nm, pH 7.0 (Hyeung-geun Park, personal communication).

Construction of Mutant DHFRs. Standard DNA procedures were followed as described (*18*). The overlap extension technique was employed to substitute Asp122 with asparagine, serine, and alanine (*19*). The expression plasmid, pET22b-DHFR (provided courteously by C. E. Cameron), was used as a template for the first polymerase chain reaction (PCR). Relevant primers are listed in Table 1. In brief, two independent PCR reactions were conducted: one reaction with the DHFR-For and the mutagenic reverse primers; the other reaction with the mutagenic forward and DHFR-Rev primers. The resulting products were gel-purified and then used in a subsequent amplification employing the DHFR-For and DHFR-Rev primers. The desired expression construct was obtained by restriction digest of the mutant gene with *Cla*I and *Bam*HI and then ligation into the pET22b-DHFR vector. Sequencing of plasmid DNA to confirm the presence of the desired mutations was performed by the Nucleic Acids Facility at the Pennsylvania State University.

Enzyme Purification. Wild-type and mutant DHFRs were purified as described previously (*20, 21*). The production of dihydrofolate reductase (DHFR) utilized the *E. coli* strain BL21(DE3) cells transformed with the pET-22b-derived expression plasmid. Cells containing the pET22b-derived expression were induced with 0.4 mM IPTG and grown at 37 °C to an OD_{600} of 0.8 in NCZYM medium (Gibco-BRL)

Table 1: Primers for Site-Directed Mutagenesis of the DHFR Gene

primer	nucleotide sequence
DHFR-For	$^{5'}$GCG GGA TCC CAT ATG ATC AGT CTG ATT GCG GCG$^{3'}$
DHFR-A122N-For	$^{5'}$GTG GAA GGC AAC ACC CAT TTT CCG$^{3'}$
DHFR-A122S/A-For	$^{5'}$GTG GAA GGC $^{G}/_{T}$ CT ACC CAT TTT CCG$^{3'}$
DHFR-Rev	$^{5'}$GCG TCT AGA GGA TCC TTA ACG ACG CTC GAG GAT$^{3'}$
DHFR-A122N-Rev	$^{5'}$CGG AAA ATG GGT GTT GCC TTC CAC$^{3'}$
DHFR-A122S/A-Rev	$^{5'}$CGG AAA ATG GGT AG$^{C}/_{A}$ GCC TTC CAC$^{3'}$

containing 200 μg mL^{-1} ampicillin. After a 4 h induction at 37 °C, the cells were harvested by centrifugation at 4 °C. From the cell pellet, a lysate was prepared and loaded on a methotrexate−agarose column (Sigma). Bound DHFR was eluted with folate. Removing folate from the eluant was accomplished using a DE-52 column (Whatman). DHFR was quantitated either spectrophotometrically ($\epsilon_{280} = 0.0746$ μM^{-1} cm^{-1}) or by active-site titration with MTX (*22*). Values obtained by these methods were within 10%. A typical preparation from 1 L of cells yielded about 5 mg of protein.

Equilibrium Dissociation Constants. The dissociation constant, K_D, was measured by ligand quenching of intrinsic protein fluorescence as a function of ligand concentration using an SLM Aminco 8000 spectrofluorometer (SLM Aminco Instruments, Inc.). Typically, DHFR was added to filtered, degassed MTEN buffer at pH 7.0 in a fluorescence cuvette. Tryptophan fluorescence was monitored at 340 nm from excitation at 290 nm. The addition of ligand resulted in a fluorescence decrease. After correction for inner filter effects, the data were fit to a quadratic equation (*23*). Acceptable K_D determinations were made using concentrations of enzyme below the respective K_D values. To quantitate DHFR, the active site was titrated with MTX using fluorescence quenching as stated above. If the protein concentration exceeds the K_D value for the ligand by 10-fold, a monotonic decrease in fluorescence will be observed until the site is saturated. A fit of these data yields the concentration of active DHFR. All binding studies were performed at pH 7.0.

Steady-State Kinetic Parameters. The rate of substrate turnover under saturating amounts of H_2F and NADPH was determined by monitoring the decrease in NADPH absorbance at 340 nm ($\epsilon_{340} = 0.0132$ μM^{-1} cm^{-1}). For a typical experiment, 50 nM enzyme was preincubated with NADPH, and the reaction was initiated upon addition of H_2F. For comparative purposes, the addition of specific ligands was reversed, and the resulting k_{cat} value was measured. Concentrations of H_2F and NADPH were varied from 50 to 200 μM to ensure reaction conditions were saturating.

To measure the reverse reaction, the same signal corresponding to NADPH was monitored, except under these conditions NADPH is being produced. Due to the high instability of tetrahydrofolate, attempts were made to minimize contact of H_4F with oxygen, light, and temperatures greater than 4 °C. As a precaution, 5 mM DTT was added to all solutions. For a typical experiment, enzyme (0.1 μM) was preincubated with 2 mM NADP$^+$, and the reaction was initiated upon addition of 100 μM H_4F. Ligand concentrations were varied to ensure saturation of enzyme.

Transient Kinetics. Transient binding and pre-steady-state kinetic experiments were performed on a stopped-flow instrument (Applied Photophysics Ltd.). Ligand binding and competition rates were measured by following quenching of intrinsic enzyme fluorescence. Enzyme tryptophans were excited at 290 nm, resulting in fluorescence at 340 nm through a 305 nm output filter. The addition of ligand quenched the fluorescence, resulting in the measured signal. Design of these experiments was based on principles discussed elsewhere (*5*, *24*, *25*). Pre-steady-state rates were measured by monitoring coenzyme fluorescence at 450 nm through a 400 nm output filter. This technique relies on excitation of enzyme tryptophans at 290 nm, which subsequently emit at 340 nm, the absorbance band for the nicotinamide ring of reduced cofactor. In a typical single-turnover experiment, DHFR (20 μM) was preincubated with limiting amount of NADPH (18 μM) in MTEN at pH 7.0, 25 °C. The addition of a saturating amount of H_2F (100 μM) resulted in a curve, which could be fit to a single exponential. The use of NADPD as a cofactor resulted in an isotope effect on the single-exponential rate, the chemistry step, of 2.8−3.0. Differences in experimental design for the mutants are discussed in detail in the Results and Discussion section.

RESULTS AND DISCUSSION

The DHFR catalytic cycle relies on the modulation of ligand specificity to regenerate the enzyme for a subsequent round of catalysis. X-ray crystallographic data indicate that alternating Met20 loop conformations play a key role in determining ligand affinity and that interloop interactions provide stabilizing contacts for either the closed or occluded Met20 loop conformations (*1*). Here, we assessed the significance of the hydrogen bond observed in the closed Met20 loop conformation involving the side chain of Asp122 in the βF−βG loop and the backbone amide of Glu17 in the Met20 loop. Substitution of side chains with weaker hydrogen-bond donors decreases the affinity for cofactor and reduces the rate of hydride transfer. Surprisingly, negative cooperativity between NADPH and H_4F is lost, such that the off rates of H_4F from the binary and mixed ternary complexes contribute to the rate of catalysis in the steady state. These mutational effects support the mechanistic model of alternate Met20 loop conformations determining ligand specificity.

Thermodynamic Binding of Ligands. The role of Asp122 in stabilizing binary complexes is minor with the exception of NADPH, as shown with K_D values for a series of mutant enzymes in Table 2. The affinity for the reduced cofactor decreases 3−4-fold, whereas binding of the oxidized cofactor is not affected. The structural difference between these forms of the cofactor resides in the nicotinamide ring, thus the observed effects indicate a loss of binding contacts to the nicotinamide ring. As predicted from the closed Met20 loop model, decreasing the ability of Asp122 to hydrogen-bond with the Met20 loop backbone decreases cofactor binding.

Table 2: K_D Values of Ligands for Wild-Type and Asp122 Mutant DHFRs at 25 °C in MTEN at pH 7.0

	K_D (μM)			
ligand	wild type[a]	Asp122Asn	Asp122Ser	Asp122Ala
MTX	<0.01	<0.01	<0.01	<0.01
NADPH	0.33 ± 0.06	0.92 ± 0.07	1.1 ± 0.1	1.3 ± 0.2
H_2F	0.22 ± 0.06	0.38 ± 0.02	0.37 ± 0.03	0.39 ± 0.02
$NADP^+$	22 ± 4	22 ± 2	22 ± 2	26 ± 3
H_4F	0.10 ± 0.01	0.098 ± 0.006	0.089 ± 0.005	0.073 ± 0.005

[a] Taken from Fierke et al. (*5*).

Table 3: Ligand k_{off} Values from Wild-Type and Asp122 Mutant DHFR Complexes at 25 °C in MTEN at pH 7.0

			k_{off} (s^{-1})			
ligand	enzyme species	trap	wild type[a]	Asp122Asn	Asp122Ser	Asp122Ala
NADPH	E·H_4F·NADPH	$NADP^+$	85 ± 10	106 ± 9	147 ± 15	153 ± 19
$NADP^+$	E·H_4F·$NADP^+$	NADPH	200 ± 20	>500	>500	>500
H_2F	E·H_2F·DNADPH	MTX	20.0 ± 0.5	10.2 ± 0.2	10.3 ± 0.2	11.1 ± 0.2
H_4F	E·H_4F	MTX	1.4 ± 0.2	3.38 ± 0.04	3.17 ± 0.03	2.65 ± 0.02
	E·H_4F·NADPH		12 ± 2	5.7 ± 0.1	4.9 ± 0.1	3.5 ± 0.1

[a] Taken from Fierke et al. (*5*).

Dissociation Rate Constants for Ligands. By employing the competition method, dissociation rate constants could be obtained for ligands from all Asp122 mutant DHFR complexes (*26*). In this technique, a saturated binary complex (E·L_1) and a large excess of a second ligand (L_2) are combined. The second ligand competes for free enzyme to yield a signal dependent on the difference in fluorescence quenching by the two ligands (Scheme 1). If $k_1[L_1] \ll k_2[L_2] \gg k_{-1}$, then the observed rate (k_{obs}) is the dissociation rate constant for L_1 (k_{-1} or k_{off}). The independence of k_{obs} on ligand concentrations confirms this conclusion.

Scheme 1

$$E\cdot L_1 \underset{k_1}{\overset{k_{-1}}{\rightleftharpoons}} E + L_1$$

$$E + L_2 \underset{k_{-2}}{\overset{k_2}{\rightleftharpoons}} E\cdot L_2$$

Modulating the hydrogen-bonding ability of Asp122 affects the ligand off rates from both substrate and product complexes in directions not predicted by the model (Table 3). To determine the off rate of H_2F from the Michaelis complex, DHFR·NADPH·H_2F, the NADPH analogue, DNADPH, was used. The off rate of substrate from the DHFR·DNADPH·H_2F complex drops 2-fold upon loss of the negatively charged side chain. This lower rate is common to all Asp122 mutants. The slight effect on the off rate of substrate from the Michaelis complex, as well as on the K_D for the binary complex, indicate a minor role for Asp122 in coordinating binding of the folyl substrate.

A more significant effect is observed with product complexes. Attempts to determine the off rate of $NADP^+$ from the DHFR·$NADP^+$·H_4F complex failed as a result of no detectable signal for all Asp122 mutants. Since the corresponding wild-type rate occurs rapidly (200 s^{-1}), it is assumed that the Asp122 mutations increase the off rate of the oxidized cofactor at least 2.5-fold (>500 s^{-1}), making the signal unobservable. The substitution of Asp122 with asparagine increases the off rate of H_4F from the DHFR·H_4F complex 2.4-fold relative to the wild-type rate. Nevertheless, increasing the loss of interloop interactions by subsequent substitutions incapable of hydrogen bonding results in a 1.3-fold decrease in this product off rate, compared to Asp122Asn DHFR. For the DHFR·NADPH·H_4F complex, loss of hydrogen-bonding ability of the 122 side chain results in increased off rates for cofactor and decreased off rates for tetrahydrofolate. The most extreme substitution, replacement of Asp122 with alanine, demonstrates a 1.8-fold increase in the off rate for NADPH and a 1.6-fold decrease in the off rate for H_4F relative to Asp122Asn DHFR values. These data suggest that the side chain of Asp122 also influences the stability of the occluded Met20 loop conformation occurring in product complexes.

Steady-State Kinetics. At pH 7.0, the rate-limiting step in the catalytic cycle of wild-type DHFR is not the rate of substrate reduction (220 s^{-1}) but rather the product off rate (12 s^{-1}) from a mixed ternary complex (DHFR·NADPH·H_4F) (*5*). The previous ligand-binding experiments shed light on key components of this cycle, namely, the liganded complexes. Another important element of this cycle is the rate of hydride transfer, which for these mutants becomes important in the flux of substrate, as evidenced by the increasing expression of an isotope effect in the steady-state rate. As a result of the mutations, hydride transfer becomes partially rate-limiting in the steady state.

Under saturating substrate (100 μM) and cofactor (100 μM), the Asp122 mutants demonstrate a partial isotope effect in the steady state at pH 7.0 (Table 4), indicating that the rate of the chemical step contributes to the steady-state rate. In the wild-type cycle, the off rate for the folyl product from the DHFR·NADPH·H_4F complex limits turnover. For the Asp122 mutants, the off rates of tetrahydrofolate from the DHFR·H_4F and DHFR·NADPH·H_4F complexes are comparable; thus both contribute to the observed rate in the steady state. The partial isotope effect suggests that the hydride transfer rate is of the same order of magnitude as these off rates. These data further support the necessity of the βF−βG loop to coordinate the appropriate conformation of the Met20, in this case, to effectively orient substrate and cofactor for hydride transfer.

Table 4: Steady-State Rates for Wild-Type and Asp122 Mutant DHFRs at 25 °C in MTEN at pH 7.0

	wild type[a]		Asp122Asn		Asp122Ser		Asp122Ala	
parameter	measured	calculated	measured	calculated[b]	measured	calculated[b]	measured	calculated[b]
k_{cat} (s^{-1}) for NADPH	12.3 ± 0.7	11.5	4.4 ± 0.4	4.5	3.3 ± 0.3	3.4	2.5 ± 0.2	2.5
k_{cat} (s^{-1}) for NADPD	10 ± 1	11.5	2.6 ± 0.2	2.8	2.0 ± 0.2	2.0	1.3 ± 0.1	1.3
k_{cat} (s^{-1}) for ^{D}V	1.1 ± 0.1	1.0	1.6 ± 0.2	1.6	1.8 ± 0.2	1.7	1.9 ± 0.3	1.9

[a] Taken from Fierke et al. (*5*). [b] See Summary of Partial Kinetic Scheme.

Table 5: Single-Turnover Rates for Wild-Type and Asp122 Mutant DHFRs at 25 °C in MTEN at pH 7.0

parameter	wild type[a]	Asp122Asn	Asp122Ser	Asp122Ala
k_b (s^{-1}) for NADPH	220 ± 10	9.4 ± 0.7	5.9 ± 0.3	4.0 ± 0.1
k_b (s^{-1}) for NADPD	78 ± 5	3.3 ± 0.3	2.2 ± 0.1	1.3 ± 0.1
k_b (s^{-1}) for ^{D}V	2.9 ± 0.2	2.8 ± 0.3	2.7 ± 0.2	3.0 ± 0.2

[a] Taken from Fierke et al. (*5*).

Pre-Steady-State Kinetics. As employed in the ligand-binding experiments, stopped-flow fluorescence permits the measurement of rapid-phase kinetics. At pH 7.0, the wild-type hydride transfer rate is much greater than the steady-state rate, 220 s^{-1} versus 12 s^{-1}. The rapid rate of hydride transfer can be obtained under pre-steady-state conditions. Unlike the ligand-binding studies, the measured signal derives from the spectral overlap of enzyme fluorescence at 340 nm with the absorbance of the reduced nicotinamide ring for NADPH. The resulting excited cofactor emits at 450 nm. This fluorescence signal decreases as substrate and cofactor turnover. Under single-turnover conditions, where one ligand is limiting, a single-exponential decay of fluorescence is observed. In a typical experiment, 18 μM NADPH was preincubated with 20 μM DHFR and the reaction was initiated upon addition of 100 μM H_2F. Substitution of NADPH with the deuterated cofactor, NADPD, results in an isotope effect of 3.0, which confirms the observed rate as hydride transfer.

Consistent with the predictions from the steady-state data, the Asp122 substitutions decrease hydride transfer rates, as a function of the ability of the side chain to interact with the Met20 loop. To avoid contributions from ligand binding, the rates for hydride transfer step were determined under single-turnover conditions and are shown in Table 5. Loss of Asp122 contacts results in a 25−55-fold reduction in the rate of this step. Hydride transfer, however, is not abolished; thus stabilizing contacts still exist, such as the backbone−backbone contacts between the βF−βG and Met20 loops. Notably, for the Asp122 mutants the rates of hydride transfer are similar to their respective product off rates (Table 3), so that the hydride transfer rates contribute more to the rate of steady-state turnover, consistent with the increasing isotope effect in the steady state.

Determining K_{eq} for Hydride Transfer. Decreased hydride transfer rates for all mutants are consistent with destabilization of the closed Met20 loop conformation. If the occluded conformation only occurs in product complexes, then the reverse rate of hydride transfer should not be affected by these mutations. Attempts to obtain this rate for the Asp122 mutants proved unsuccessful at pH 7.0 (data not shown). Nevertheless, due to the pH dependence of hydride transfer, the wild-type rate of hydride transfer is rate-limiting under steady-state conditions at pH 9.0. In fact, the reverse rate of hydride transfer is optimal at pH 9.0, occurring at 0.6 s^{-1} (*5*). To assess the effects of the βF−βG loop mutations on the rate of hydride transfer, catalysis in both directions was determined for the Asp122 mutants at pH 9.0. The forward hydride transfer rate was measured as described previously under Steady-State Kinetics. To measure the reverse rate of hydride transfer, the reaction was initiated upon addition of 50 μM H_4F to 0.5 μM DHFR preincubated with 2 mM $NADP^+$ and the resulting increase in absorbance at 340 nm (NADPH) was monitored.

Surprisingly, the steady-state rates in both the forward and reverse direction for the Asp122 mutants at pH 9.0 decrease as a function of weakening the βF−βG and Met20 loop contacts by side-chain substitution (Table 6). The overall K_{eq} values shift to favor the forward reaction, where H_4F is produced. There are two important implications from these results. First, the similarity of the trends in both directions indicates the importance of the βF−βG loop in determining the transition state for hydride transfer to occur. Nevertheless, it is unclear when the Met20 loop converts from the closed conformation to the occluded conformation. If this conformational change occurs after chemistry, then the closed Met20 loop conformation is the only catalytically competent form of the loop. Perturbations of the closed conformation would affect the hydride transfer rate in both directions, as observed with these mutants. Second, the equilibrium shift favoring the DHFR·$NADP^+$·H_4F complex underscores the importance of the interloop contacts to modulate the Met20 loop conformational change to distinguish between substrate and product complexes.

Summary of Partial Kinetic Scheme. Determination of the ligand K_D values (Table 2), ligand dissociation rate constants (Table 3), and rates of substrate conversion (Tables 4 and 5) enables the construction of a partial kinetic scheme for the Asp122 mutants at pH 7.0. For simplicity, only the partial kinetic scheme for Asp122Ala DHFR is shown (Scheme 2). The value of k_{on} for H_4F to apoenzyme was calculated from the k_{off} value and the respective K_D value by the relationship with k_{off}/k_{on}. There are two striking features common to the Asp122 mutant kinetic schemes.

First, substitution of the acid side chain significantly decreases the rate of hydride transfer. The effects of the Asp122 mutants on the rate of hydride transfer demonstrate the sensitivity of the formation of the Michaelis complex to the interloop interactions. Substitution of the acid side chain by neutral residues ultimately weakens binding interactions with the nicotinamide ring without appreciably affecting substrate binding. The effects on cofactor binding are coincident with decreases in hydride transfer. In fact, a logarithmic plot of the affinity for NADPH (reciprocal of the K_D value, Table 2) versus the rate of hydride transfer can be fitted to a linear regression with a significant correlation coefficient ($R = 0.998$), as shown in Figure 2.

Table 6: Steady-State Rates for Wild-Type and Asp122 Mutant DHFRs at 25 °C in MTEN at pH 9.0

parameter	wild type	Asp122Asn	Asp122Ser	Asp122Ala
k_{cat} (s^{-1}) forward	3.0 ± 0.2	0.26 ± 0.02	0.22 ± 0.02	0.13 ± 0.01
k_{cat} (s^{-1}) reverse	0.6 ± 0.1	0.019 ± 0.002	0.012 ± 0.001	0.0044 ± 0.0002
K_{eq} (k_{for}/k_{rev})	5 ± 1	14 ± 1	18 ± 1	30 ± 2

Scheme 2: Partial Kinetic Scheme for Asp122Ala DHFR at 25 °C in MTEN at pH 7.0[a]

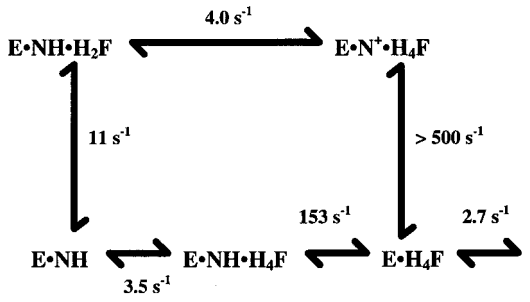

[a] NH = NADPH; N^+ = $NADP^+$; H_2F = dihydrofolate; H_4F = tetrahydrofolate.

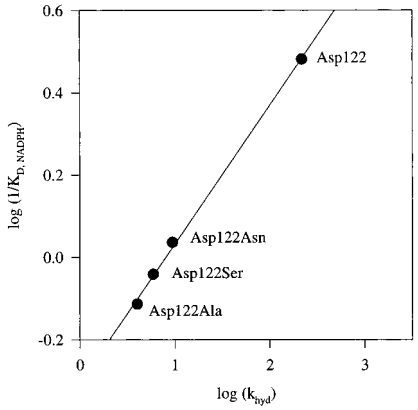

FIGURE 2: Correlation of NADPH affinity and the hydride transfer rate. The log of cofactor affinity for wild type and the Asp122 mutants as determined by the reciprocal of the K_D value (Table 2) is plotted against the log of the hydride transfer rate. These resulting data were fit to a linear regression to yield a slope of 2.97 ± 0.08, a *y*-intercept of 0.90 ± 0.02, and a correlation coefficient of 0.998.

The implications of the large slope (ca. 3) are unclear. Nevertheless, the linearity of the curve indicates that the interactions of Asp122 are along the reaction coordinate leading to the transition state. The pronounced effects on the rate of hydride transfer likely derive from perturbed binding of the nicotinamide ring. The angle and distance between hydride donor and acceptor have been shown to be critical for a hydride transfer reaction by isocitrate dehydrogenase (*27*) and in the *ab initio* calculations for hydride transfer (*28*).

Second, substitutions for Asp122 alter the catalytic pathway preferred by wild-type DHFR under saturating conditions of substrate and cofactor. In the wild-type mechanism, the enzyme cycles through five kinetically observable intermediates highlighted in boldface type (Scheme 2). The trend in the Asp122 mutants is to shift the internal equilibrium to favor the DHFR·$NADP^+$·H_4F product complex as the hydrogen-bonding ability of the substituted amino acid decreases. In addition, the rapid loss of oxidized cofactor is facilitated. With comparable product off rates from either the DHFR·H_4F or DHFR·NADPH·H_4F complexes owing to the reduced negative cooperativity relative to DHFR·NADPH·H_4F in the wild-type enzyme (*5*), the release of product partitions between the two complexes depending on the NADPH concentration to a greater degree for the mutant DHFRs. Taken together, the rate of steady-state catalysis contains contributions from the off rates of product from both complexes and from the rate of hydride transfer.

The magnitude of the mutational effects on the kinetic pathway increases as the hydrogen-bonding ability of the 122 side chain decreases. The substitution of Asp122 with asparagine does not affect the K_D value for H_4F. Since the off rate for product from the binary complex increases 2.4-fold compared to the wild-type rate, the on rate for this ligand must also increase 2.4-fold. In other words, exchange of the charged side chain for a polar side chain increases the rate of attainment of equilibrium in the product complex. The formation of a weaker hydrogen bond between the Met20 and βF−βG loops apparently facilitates the binding and release of H_4F. As the 122 side chain is substituted with serine, a weaker hydrogen-bond former, or alanine, incapable of forming hydrogen bonds, the K_D value for H_4F decreases. These findings are consistent with a favoring of the occluded Met20 loop conformation, as a result of a destabilized closed Met20 loop conformation derived from the Asp122 substitutions.

A good test of the validity of the kinetic schemes for the Asp122 mutants is a comparison of the measured steady-state rates with those predicted by this model. The simulation of the Asp122 mutant DHFR mechanisms using KINSIM (*29*) required two assumptions. Since the test conditions involve saturating conditions of H_2F (100 μM) and NADPH (100 μM), the ligand on rates would be very high. Compared to wild-type values, the effects of the Asp122 mutations are manifest mainly in ligand off rates (Table 3). With these considerations, a value of 1000 s^{-1} was used as the on rate for these ligands, a value at least 2-fold less than the corresponding wild-type values. For the reverse chemistry reaction, the wild-type rate is not measurable, so a lower limit based on the assay conditions was used (0.003 s^{-1}). Taken together, the calculated steady-state rates are within error of measured values, including the partial isotope effect derived from the contributions of the hydride transfer rate (Table 4). Consequently, the identical kinetic sequence describes the behavior of the Asp122 mutants, although the values of the individual steps have been altered. These findings further support the role of the βF−βG loop as a guiding loop in the formation of all DHFR complexes, including a role in the mechanism of negative cooperativity between H_4F and NADPH observed in the wild-type kinetic scheme.

Dynamics of the Met20 Loop. On the basis of X-ray crystallographic data, Sawaya and Kraut proposed that the Met20 loop of DHFR modulates ligand specificity by adopting either of two conformations (*1*). Key stabilizing contacts for these conformations involve networks of hy-

drogen bonds with outside loops. Specifically, a closed Met20 conformation occurring in substrate complexes (DHFR·NADPH and DHFR·NADPH·H_2F) relies on interactions with the βF−βG loop, whereas the occluded conformation occurring in product complexes (DHFR·$NADP^+$·H_4F, DHFR·H_4F, and DHFR·NADPH·H_4F) entails interactions with the βG−βH loop. To test the validity of this model, we targeted the hydrogen bond between the side chain of Asp122 in the βF−βG loop and the amide backbone of Glu17 in the Met20 loop for mutagenesis to weaken the strength of this bond.

Surprisingly, the substitutions of Asp122 perturb all liganded complexes (Summary of Partial Kinetic Scheme). Either the βF−βG loop affects the formation of a different Met20 loop occurring in product complexes or the closed conformation contributes to product complexes. In the absence of structural data, it is not possible to differentiate between these two possibilities; however, an equilibrium between the closed and occluded Met20 loop conformations in liganded complexes may explain the data observed for the Asp122 mutants. In this model, side-chain exchange for Asp122 results in a shift of the Met20 loop equilibrium to favor the occluded conformation in which the middle portion of the Met20 loop (Glu17−Met20) occupies part of the nicotinamide binding site for cofactor, thereby inhibiting cofactor binding. Indeed, the DHFR·NADPH complex is less stable (higher K_D values) and cofactor off rates increase from respective liganded complexes. Moreover, a higher population of the occluded conformation favors tetrahydrofolate binding in forming the binary product complexes, as evidenced by decreasing K_D values as the substituted amino acid becomes a poorer hydrogen-bond donor. The tighter binding derives from an unexpected, apparent increase in the association rates for tetrahydrofolate that more than compensates for the increased off rates.

Concluding Remarks. Enzymes are known to undergo a variety of conformational changes; nevertheless, demonstrating how these dynamics contribute to catalysis is difficult. The static window into the DHFR catalytic cycle provided by X-ray crystallographic data indicates two Met20 conformations (closed and occluded) exist in liganded complexes (*1*). The contributions of this study emphasize the importance of the βF−βG loop modulating Met20 conformations. The data from the Asp122 mutants suggest that these loops interact transiently to affect the formation of all liganded complexes, likely through an equilibrium of closed and occluded Met20 conformations dependent on bound ligands and interloop interactions. Thus, a kinetic analysis of mutants generated from site-directed mutagenesis serves to illustrate a dynamical aspect of catalysis not readily apparent from X-ray crystal structures.

REFERENCES

1. Sawaya, M. R., and Kraut, J. (1997) *Biochemistry 36*, 586−603.
2. Falzone, C. J., Benkovic, S. J., and Wright, P. E. (1990) *Biochemistry 29*, 9667−9677.
3. Falzone, C. J., Wright, P. E., and Benkovic, S. J. (1994) *Biochemistry 33*, 439−442.
4. Epstein, D. M., Benkovic, S. J., and Wright, P. E. (1995) *Biochemistry 34*, 11037−11048.
5. Fierke, C. A., Johnson, K. A., and Benkovic, S. J. (1987) *Biochemistry 26*, 4085−4092.
6. Cannon, W. R., Garrison, B. J., and Benkovic, S. J. (1997) *J. Am. Chem. Soc. 119*, 2386−2395.
7. Cleland, W. W. (1975) *Acc. Chem. Res. 8*, 145.
8. Appleman, J. R., Beard, W. A., Delcamp, T. J., Prendergast, N. J., Freisheim, J. H., and Blakely, R. L. (1990) *J. Biol. Chem. 265*, 2740−2748.
9. Bystroff, C., and Kraut, J. (1991) *Biochemistry 30*, 7826−7833.
10. Blakely, R. L. (1960) *Nature (London) 188*, 231−232.
11. Mathews, C. K., and Huennekens, F. M. (1960) *J. Biol. Chem. 235*, 3304−3308.
12. Viola, R. E., Cook, P. F., and Cleland, W. W. (1979) *Anal. Biochem. 96*, 334−340.
13. Branlant, G., Eiler, B., and Biellmann, J. F. (1982) *Anal. Biochem. 125*, 264−268.
14. Dawson, R. M. C., Elliot, D. C., Elliot, W. H., and Jones, K. M. (1969) *Data for Biochemical Research*, p 199, Oxford University Press, Oxford, U.K.
15. Kallen, J. R., and Jencks, W. P. (1968) *J. Biol. Chem. 241*, 5845−5850.
16. Seeger, D. R., Cosulich, D. B., Smith, J. M., and Hultquist, M. E. (1949) *J. Am. Chem. Soc. 71*, 1753−1758.
17. P-L Biochemicals (1961) *Circular OR-18*, P-L Biochemicals, Milwaukee, WI.
18. Sambrook, J., Fritsch, E. F., and Maniatis, T. (1989) *Molecular Cloning: A Laboratory Manual*, Cold Spring Harbor Laboratory Press, Cold Spring Harbor, NY.
19. McPherson, M. J., Quirke, P., and Taylor, G. R. (1991) *PCR: A Practical Approach*, Oxford University Press, Oxford, U.K.
20. Cameron, C. E., and Benkovic, S. J. (1998) *Biochemistry* (in press).
21. Miller, G. P., and Benkovic, S. J. (1998) *Biochemistry* (in press).
22. Williams, J. W., Morrison, J. F., and Duggleby, R. G. (1979) *Biochemistry 18*, 2567−2573.
23. Taira, K., and Benkovic, S. J. (1988) *J. Med. Chem. 31*, 129−137.
24. Velick, S. F. (1958) *J. Biol. Chem. 233*, 1455−1467.
25. Dunn, S. M. J., and King, R. W. (1980) *Biochemistry 19*, 766−773.
26. Birdsall, B., Burgen, A. S., and Roberts, G. C. K. (1980) *Biochemistry 19*, 3723−3731.
27. Mesecar, A. D., Stoddard, B. L., and Koshland, D. E. (1997) *Science 277*, 202−206.
28. Benkovic, S. J., Fierke, C. A., and Naylor, A. M. (1988) *Science 239*, 1105−1109.
29. Barshop, B. A., Wrenn, R. F., and Frieden. C. (1983) *Anal. Biochem. 130*, 134−145.

BI973065W